

# How lime-sand islands in the South China Sea have responded to global warming over the last 30 years: Evidence from satellite remote sensing images

Jialiu Liu<sup>a,b,c,1</sup>, Rongyong Huang<sup>a,b,c,1</sup>, Kefu Yu<sup>a,b,c,\*</sup>, Bin Zou<sup>d,e</sup>

<sup>a</sup> Guangxi Laboratory on the Study of Coral Reefs in the South China Sea, Guangxi University, Nanning 530004, China

<sup>b</sup> Coral Reef Research Centre of China, Guangxi University, Nanning 530004, China

<sup>c</sup> School of Marine Sciences, Guangxi University, Nanning 530004, China

<sup>d</sup> Southern Marine Science and Engineering Guangdong Laboratory (Guangzhou), China

<sup>e</sup> National Satellite Ocean Application Service, Beijing 100081, China

## ARTICLE INFO

### Article history:

Received 8 March 2020

Received in revised form 3 September 2020

Accepted 7 September 2020

Available online 11 September 2020

### Keywords:

Lime-sand islands

Coral reefs

Areal changes

Global warming

Satellite image analysis

South China Sea

## ABSTRACT

As global warming threatens their existence, there are widespread concerns regarding the persistence of lime-sand islands and the future of mid-ocean atoll nations. To investigate how climate change has affected lime-sand islands, changes in vegetation and other characteristics of such islands in the South China Sea (SCS) were investigated from 1989 to 2019 using 67 satellite images. First, boundaries of the lime-sand islands and their vegetation were extracted using an active contour extraction procedure called the gradient vector flow snake model. Afterwards, the spatial extents were estimated by enclosing the extracted boundaries, and the digital shoreline analysis system was used to calculate beach widths. Finally, area growth rates and speeds were used to evaluate areal changes in the lime-sand islands and their respective vegetation. Based on the estimated area growth rates, area growth speeds, and beach widths, the lime-sand islands in SCS eroded over the past three decades whereas their vegetation expanded. Further analysis suggested that direct inundation caused by sea-level rise might not be clearly identified from the satellite images. However, other climate change-related factors were most likely responsible for the observed island erosions. These factors included higher wave energy, stronger typhoon intensity and destructiveness, and accelerated coral reef degradation. In addition, the observed expansion of vegetation on the lime-sand islands was likely due to the increase in precipitation in a warming world. The results show that 1) the lime-sand islands will continue to erode whereas vegetation will continue to expand; 2) As vegetation growth is significantly inhibited by salt water when it is adjacent to the ocean, vegetation areas on lime-sand islands may start to continuously decline. Overall, this study is the first to quantitatively examine changes in SCS lime-sand islands due to global warming.

© 2020 Elsevier B.V. All rights reserved.

## 1. Introduction

Coral reefs and islands make up the majority of the populated landmass in certain Pacific and Indian Ocean nations (Ford, 2012). They are composed of largely unconsolidated reef-derived sediments (Stoddart and Steers, 1977) and are vulnerable to climate change (Woodroffe, 2008). Due to their low elevation, unconsolidated sediments, small areal extent, climate change sensitivity, and

high population densities, there are serious concerns regarding the persistence of these lime-sand islands and the future of these mid-ocean atoll nations (McLean and Kench, 2015).

Lime-sand islands face the possibility of sinking in the future due to sea-level rise (Connell, 2003; Dickinson, 2009; IPCC, 2018) and are very affected by sea flooding and shoreline erosion (Mimura, 1999; Woodroffe, 2008; Terry and Chui, 2012). In addition, global warming has caused the strongest tropical cyclones to become more intense (Kossin et al., 2013, 2020) which leads to increased frequency of storm-surge-related floods. Furthermore, ocean warming and acidification induced by global warming have degraded coral reefs (Hoegh-Guldberg et al., 2007; Fabricius et al., 2011), which reduces bottom friction and leads to greater wave heights, higher wave run-up, and more wave-driven flooding (Quataert et al., 2015; Storlazzi et al., 2015). As a result, residents of coral reefs and islands have been generally regarded as the first climate change refugees in the world (Barnett, 2005; McAdam, 2010).

*Abbreviations:* DSAS, Digital Shoreline Analysis System; SCS, South China Sea; WLR, weighted linear regression; GVF, gradient vector flow; LWM, low water mark; ToB, toe of the beach; SCE, Shoreline Change Envelope; PDI, power dissipation index; STY, strong typhoons; SuperTY, super typhoons.

\* Corresponding author at: Coral Reef Research Centre of China, Guangxi University, Nanning 530004, China.

E-mail addresses: [kefuyu@gxu.edu.cn](mailto:kefuyu@gxu.edu.cn), [kefuyu@scsio.ac.cn](mailto:kefuyu@scsio.ac.cn) (K. Yu).

<sup>1</sup>These authors contributed equally to this study.

Previous studies have demonstrated examples of decrease in lime-sand island area over the past several decades. For example, [Houser et al. \(2014\)](#) indicated that the Sapodilla Cays of the Mesoamerican Barrier Reef have eroded since the 1960s, wherein certain lime-sand islands in that region have lost 70% of their area. [Romine and Fletcher \(2013\)](#) showed that the shorelines of Kauai, Oahu, and Maui (Hawaii) suffered 70% erosion to beaches, including 9% that was completely lost to erosion, e.g., seawalls. However, additional studies on island changes have revealed different results. For example, the areas of certain lime-sand islands in the western and central Pacific were determined to be stable or even slightly increasing ([Webb and Kench, 2010](#); [Ford and Kench, 2015](#); [McLean and Kench, 2015](#)). All these studies evaluated the period of strong climate warming over the past few decades and considered factors such as sea-level rise and typhoon damage. Therefore, observed dynamic changes of lime-sand islands due to climate change exhibit different response patterns in different regions. Consequently, extensive research is necessary to analyse how specific lime-sand islands respond to global warming.

The South China Sea (SCS) is the largest semi-enclosed marginal sea in the northwest Pacific ([Liu et al., 2010](#); [Deng et al., 2013](#)). There are hundreds of coral reefs and islands in the SCS ([Morton and Blackmore, 2001](#)), making the region ideal for studying climate-related changes ([Talaue-McManus, 2000](#); [Burke et al., 2002](#); [Yu, 2012](#)). However, data limitations and distance from the mainland have made analysing trends in the region difficult ([National Marine Information Center, 2017](#); [Liu et al., 2020](#)). However, satellite remote sensing has made it possible to assess changes to the coral reefs and islands over the past several decades ([Fletcher et al., 2003](#); [Huang et al., 2017, 2018](#); [Behling et al., 2018](#)).

This study focusses on the changes to lime-sand islands in the SCS over the past three decades based on multi-decadal Landsat and

Sentinel-2 images. We propose a new strategy to use satellite images to detect changes to lime-sand islands, mitigating SCS data limitation issues. Furthermore, we provide new insights into how the lime-sand islands have responded to global warming, helping us predict the future of these coral reefs and islands.

## 2. Materials and methods

### 2.1. Regional setting

In the SCS, there are hundreds of coral reefs including islands, banks, and shoals ([Morton and Blackmore, 2001](#)). To study how lime-sand islands have responded to global warming, we focussed on several natural lime-sand islands across the central and southern SCS. These islands were chosen according to the following conditions: 1) areal extent greater than  $8 \times 10^4 \text{ m}^2$ ; 2) rarely affected by human activities, i.e. the islands contain few artificial objects such as buildings; 3) at least 10% covered by vegetation at the end of the study period. These conditions ensured that the outer boundaries and vegetation of the chosen lime-sand islands could be detected from the experimental satellite images.

For the central SCS, eight lime-sand islands in the Xisha Islands were chosen, as shown in [Fig. 1](#). They are Jinyin Island ([Fig. 1a](#)), Ganquan Island ([Fig. 1b](#)), Jinqing Island ([Fig. 1c](#)), Shanhu Island ([Fig. 1d](#)), Xishahou ([Fig. 1e](#)), Bei Island ([Fig. 1f](#)), Zhong Island ([Fig. 1g](#)), and Nan Island ([Fig. 1h](#)). For the southern SCS, the main coral reefs are shoals rather than lime-sand islands; only three lime-sand islands in the Nansha Islands could be selected. These are Beizi Island ([Fig. 1i](#)), Xiyue Island ([Fig. 1j](#)), and Mahuan Island ([Fig. 1k](#)). No lime-sand islands in the Dongsha and Zhongsha Islands met our criteria and therefore were not selected for the study.

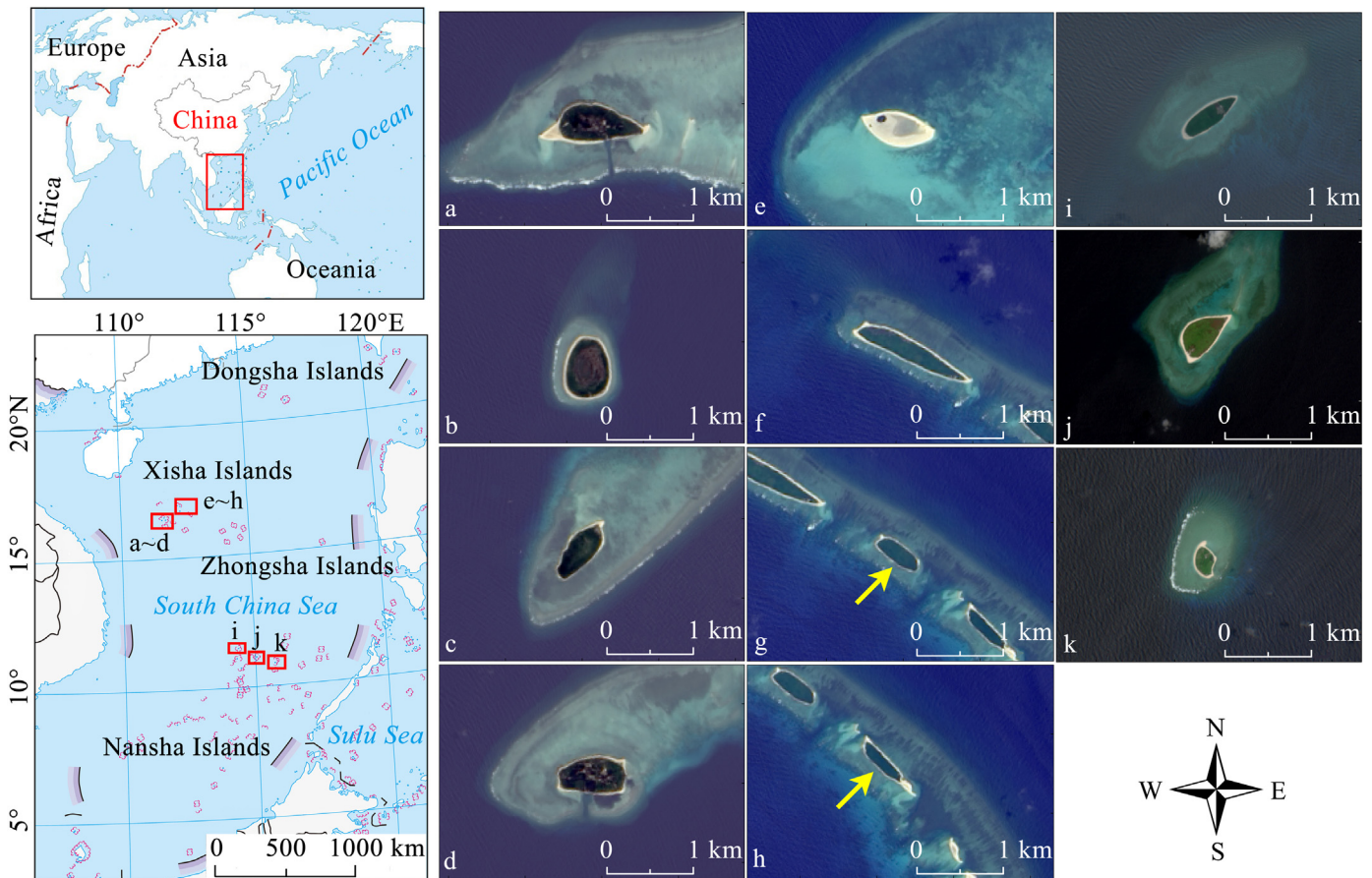


**Fig. 1.** Distribution of the studied lime-sand islands in the SCS: (a) Jinyin Island, (b) Ganquan Island, (c) Jinqing Island, (d) Shanhu Island, (e) Xishahou, (f) Bei Island, (g) Zhong Island, (h) Nan Island, (i) Beizi Island, (j) Xiyue Island, and (k) Mahuan Island. The geographical base map was downloaded from <http://bzdt.ch.mnr.gov.cn/>.

**Table 1**  
Satellite images used in this study.

Island Name	Ganquan Island	Jinqing Island	Jinyin Island	Shanhu Island	Xishazhou	Bei Island	Zhong Island	Nan Island	Beizi Island	Mahuan Island	Xiyue Island
Date and sensors	1989/4/9	1989/4/9	1989/4/9	1989/4/9	1989/6/20	1989/6/20	1989/6/20	1989/6/20		1989/6/15	
					1995/4/2	1995/4/2	1995/4/2	1995/4/2	1992/5/21	1995/5/31	1992/3/3 1995/7/18
	1996/3/3	1996/3/3	1996/3/3	1996/3/3					1998/9/3		
					1999/9/12 <sup>a</sup>	1999/9/12 <sup>a</sup>	1999/9/12 <sup>a</sup>	1999/9/12 <sup>a</sup>	1999/9/30 <sup>a</sup>	1999/2/19	2000/9/17 2001/4/21 <sup>a</sup>
	2000/8/5	2000/8/5	2000/8/5	2000/8/5							
	2002/2/24 <sup>a</sup>	2002/2/24 <sup>a</sup>	2002/2/24 <sup>a</sup>						2002/1/25 <sup>a</sup>		
				2003/1/26 <sup>a</sup>						2003/1/21 <sup>a</sup>	
	2005/3/12	2005/2/15 <sup>a</sup>	2005/3/12	2005/3/12	2004/5/4 <sup>a</sup> & 2004/12/22	2004/12/22	2004/5/4 <sup>a</sup>	2004/12/22		2005/3/14	2005/3/23 2005/4/24
					2006/3/7 <sup>a</sup> 2008/9/4 <sup>a</sup>						
	2009/5/10	2009/5/10	2009/5/10	2009/5/10	2009/4/24 2010/2/14 <sup>a</sup>	2008/9/4 <sup>a</sup> 2009/4/24	2009/4/24 2010/2/14 <sup>a</sup>	2009/4/24 2010/2/14 <sup>a</sup>	2009/3/17 <sup>a</sup>	2008/2/4 <sup>a</sup>	
			2010/2/14 <sup>a</sup>							2010/2/17 2011/4/1 <sup>a</sup>	2010/8/12
	2013/5/21 <sup>b</sup>	2013/5/21 <sup>b</sup>	2013/5/21 <sup>b</sup>	2013/5/21 <sup>b</sup>					2013/11/15 <sup>b</sup>		
					2014/6/25 <sup>b</sup> 2015/5/11 <sup>b</sup> 2016/3/21 <sup>c</sup>	2014/6/25 <sup>b</sup> 2015/5/11 <sup>b</sup>	2014/6/25 <sup>b</sup> 2015/5/11 <sup>b</sup>	2014/6/25 <sup>b</sup> 2015/5/11 <sup>b</sup> 2016/3/21 <sup>c</sup>		2015/10/20 <sup>b</sup>	2015/1/30 <sup>b</sup> 2016/3/25 <sup>c</sup>
	2015/6/28 <sup>b</sup>	2015/6/28 <sup>b</sup>	2015/6/28 <sup>b</sup>	2015/6/28 <sup>b</sup>							
	2017/3/6 <sup>c</sup>	2017/3/6 <sup>c</sup>	2017/3/6 <sup>c</sup>	2017/3/6 <sup>c</sup>					2017/5/12 <sup>c</sup>		
										2018/8/22 <sup>c</sup>	2018/5/14 <sup>b</sup>
	2019/2/24 <sup>c</sup>	2019/2/24 <sup>c</sup>	2019/2/24 <sup>c</sup>	2019/2/24 <sup>c</sup>	2019/3/21 <sup>c</sup>		2019/3/21 <sup>c</sup>	2019/3/21 <sup>c</sup>	2019/3/5 <sup>c</sup>	2019/2/26 <sup>b</sup>	2019/3/30 <sup>c</sup>

Unmarked images are taken by Landsat TM, 30-m resolution multispectral images.

<sup>a</sup> Landsat ETM+, 15-m resolution panchromatic and 30-m resolution multispectral images.

<sup>b</sup> Landsat OLI images, 15-m resolution panchromatic and 30-m resolution multispectral images.

<sup>c</sup> Sentinel-2 MSI, 10-m resolution multispectral images.

## 2.2. Experimental data

To analyse the changes in the islands, a long-term series of high-resolution images was considered ideal. However, high-resolution satellite images are expensive and did not exist for the SCS during the 20th century. As a result, we chose a series of free Landsat and Sentinel-2 images to detect long-term changes in the lime-sand islands. Cloud-free Landsat and Sentinel-2 images from 1989 to 2019 were collected and used for this study, as shown in Table 1.

A radiometric correction was performed before edge extraction of the lime-sand islands and vegetation from the satellite images. The radiometric correction includes radiometric calibration and an atmospheric correction (Chen et al., 2005). These were implemented using the radiometric calibration tool and FLAASH (Cooley et al., 2002) atmospheric correction tool of the ENVI 5.3 software. Thereafter, for Landsat OLI and Landsat ETM+ images, 30-m resolution multispectral and 15-m resolution panchromatic images were pansharpened to 15 m resolution using the Gram-Schmidt transformation (Clayton, 1971) tool of the ENVI 5.3 software. Due to the lack of a higher resolution panchromatic image, fusion was not performed for Landsat TM and Sentinel-2 MSI images; therefore, the resolution of the Landsat TM and Sentinel-2 remained 30 and 10 m, respectively.

## 2.3. Extraction of the edges of the lime-sand islands and the vegetation

Our analysis estimated the areal extents of the lime-sand islands by extracting the island edges from the satellite images. Various edge extraction methods were previously proposed to examine island changes. For example, Fletcher et al. (2003) and Romine et al. (2009) used the toe of the beach (ToB) to represent the position of the low water mark (LWM). Meanwhile, Webb and Kench (2010), Ford (2012, 2013), and Ford and Kench (2015) used vegetation lines to study the shoreline movements.

In this study, we chose to extract both the ToB and vegetation lines from the satellite images. For the SCS lime-sand islands, the ToB is the

intersection of beach sediments with the reef surface, characterised by a distinct break (Kench and Brander, 2006a, 2006b; Thomas and Hildegard, 2014). In other words, the ToB appeared as a bright-dark boundary in satellite images, enabling identification of the ToB from image tone (Thomas and Hildegard, 2014). In addition, vegetation lines were determined by identifying the boundary between the green vegetation and white beach from the true-colour satellite images.

To reduce uncertainty and improve accuracy, an active contour extraction procedure was used to extract the ToB and vegetation lines. Active contour extraction is an image line and edge feature extraction procedure in the computer vision field, first proposed by Kass et al. (1988) and often referred to as 'snake'. A snake is an energy-minimising spline guided by external constraint forces and influenced by image forces that pull it toward line and edge features. An improved snake model called gradient vector flow snake (GVF-snake) was used in this study. This method was proposed by Xu and Prince (1997), and the code (GVF 2D Matlab-Windows v5.0) was downloaded from [http://www.nitrc.org/frs/?group\\_id=271](http://www.nitrc.org/frs/?group_id=271). GVF-snake has been widely applied to high precision contour extraction, e.g. medical image processing (Xu et al., 1999; Zamani and Safabakhsh, 2007; Erkol et al., 2010) and remote sensing image processing (Song et al., 2013; Zhang et al., 2017). According to Liu et al. (2020), GVF-snake can reach a sub-pixel precision; that is, the accuracy of the localisation of a boundary detected by GVF-snake is better than 1/2 pixel for coral reef satellite images.

In this study, when the edges were observed to significantly deviate from the real ToB and vegetation lines or distraction phenomenon occurred (Cheng and Foo, 2007), manual edits were used to compensate for the deviation and distraction.

## 2.4. Calculation of area growth rates and speeds

Once the ToB and vegetation lines were extracted, the areas enclosed by the ToB and vegetation lines were calculated using ArcGIS 10.5. Specifically, the lime-sand island area was calculated by enclosing the ToB, and the vegetation area was calculated by enclosing the vegetation lines. Note that the selected lime-sand islands have rarely been

modified by human activities, so there are few buildings. As a result, the interior of the vegetation lines was nearly completely filled with vegetation. In other words, only a very few barren areas and drainage lines were found inside the vegetation lines, so the extents of the barren areas and drainage lines could be ignored. The estimated lime-sand island and vegetation areas were arranged in chronological order to form a time series. The changes to the lime-sand islands and the vegetation were then studied by examining area growth speeds and rates.

If area growth speed is positive, then the area is increasing; otherwise, the area is decreasing. We imitated the definition of velocity in Physics to express area growth speed as the following differential equation:

$$v = \frac{dS}{dt} \tag{1}$$

where  $S$ ,  $t$ , and  $v$  represent area, time, and area growth speed, respectively.

The following expression was then obtained by integrating Eq. (1):

$$S = S_0 + v(t - t_0) \tag{2}$$

or

$$S = u + vt \tag{3}$$

where  $S_0$  and  $t_0$  represent the initial area and initial time, respectively, and  $u = S_0 - vt_0$ .

According to Eq. (3), area growth speed can be estimated through a linear regression of the area ( $S$ ) on the time ( $t$ ). The coefficient  $v$  of the regression is the estimation of the area growth speed. Specifically, we used a weighted linear regression (WLR) method, where weights were chosen to be inversely proportional to the resolution of the satellite images. As the resolutions of the Landsat TM, Landsat ETM, Landsat OLI, and Sentinel-2 MSI images were 30, 15, 15, and 10 m respectively,

the weights were set as 1 ( $30 \cdot \frac{1}{30}$ ) for TM images, 2 ( $30 \cdot \frac{1}{15}$ ) for ETM+ and OLI images, and 3 ( $30 \cdot \frac{1}{10}$ ) for Sentinel-2 MSI images.

Area growth rate can be defined as the average annual percent change in the lime-sand island area or its vegetation. We imitated the Malthusian model for population growth (Haque et al., 2012) to describe the area growth rate with the following differential equation:

$$r = \frac{dS}{Sdt} \tag{4}$$

where  $r$ ,  $S$ , and  $t$  represent the area growth rate, area, and time, respectively. By integrating Eq. (4), we obtained:

$$S = S_0 e^{r(t-t_0)} \tag{5}$$

or

$$\ln S = q + rt \tag{6}$$

where  $S_0$  and  $t_0$  represent the initial area and initial time, respectively, and  $q = \ln S_0 - rt_0$ .

Similar to area growth speed, the area growth rate of a lime-sand island or its vegetation can be estimated using a WLR of  $\ln S$  on the time ( $t$ ) as well. The coefficient  $r$  of the regression estimates the area growth speed. The difference of this approach is that the logarithm of the area ( $\ln S$ ) is used instead of the area ( $S$ ) in the regression.

Note that the areas of the lime-sand islands were estimated using the ToB, and the ToB represents the position of the low water mark (LWM). As the ToB was identified using image tone, we cannot rule out the possibility that the estimated areas were influenced by tidal variations. To comprehend such possible influence, we extracted the areas of a lime-sand island (Ganquan Island) using seven Sentinel-2 MSI multispectral images. The images were captured in a short period of time (2015/11/22–2016/10/07). The lime-sand island area was considered

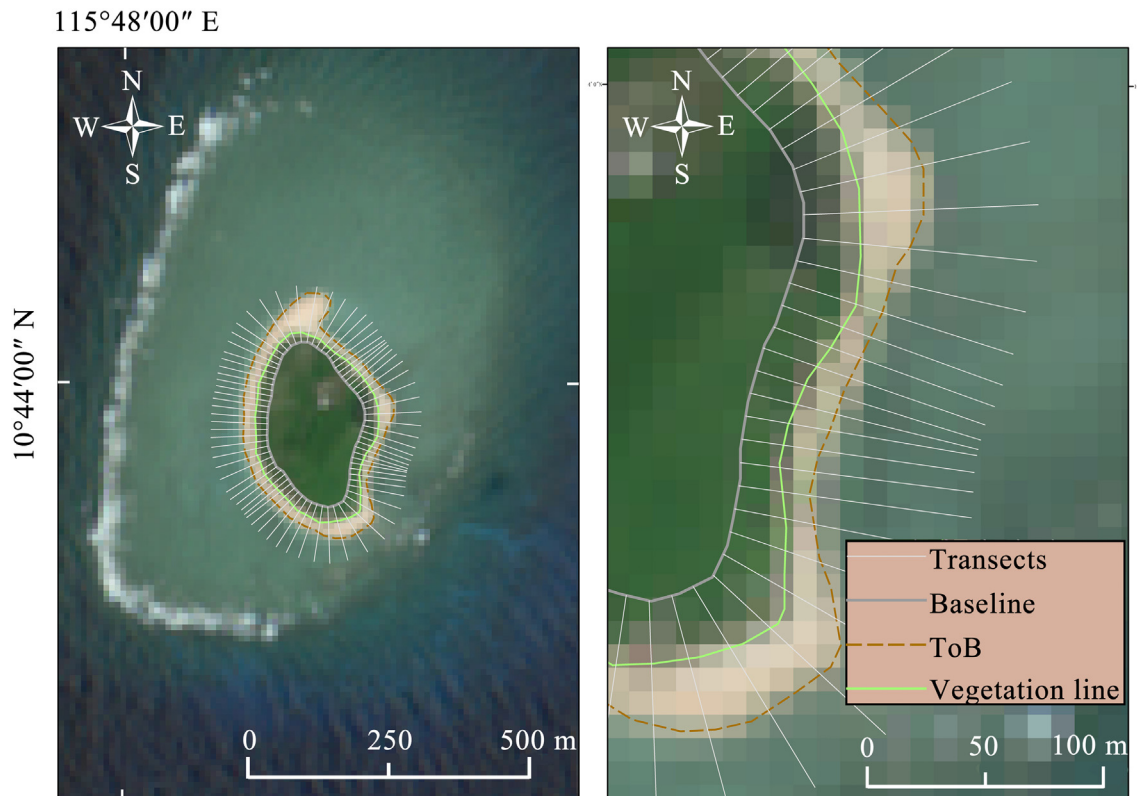


Fig. 2. SCE calculation for the beach width estimation (Mahuan Island is shown as an example).

to be invariant during the study period. The lime-sand island areas extracted from the images and the corresponding tidal levels were then drawn on a scattergraph, to evaluate the potential influence of tidal levels. Tidal level was calculated using Oregon State University's (OSU) Tidal Inversion Software, downloaded from <http://volkov.oce.orst.edu/tides/>, and results are discussed at the end of Section 3.2.

2.5. Calculation of beach widths

As beach is an important part of a SCS lime-sand island, beach width is an important attribute. Beach widths were determined using the average distance between the ToB and vegetation lines. They were

calculated using the Digital Shoreline Analysis System (DSAS 5.0) (Himmelstoss et al., 2018).

DSAS 5.0 is a software extension for ArcGIS 10.5 that examines the positional changes of shorelines (Ford, 2013). Specifically, the Shoreline Change Envelope (SCE) statistic was used to estimate the beach widths. SCE represents the distance between the farthest and closest shoreline from the baseline at a transect (Himmelstoss et al., 2018). To estimate the beach widths, we treated the ToB and vegetation line as two different shorelines, and created a baseline inside the vegetation line for each of the lime-sand islands. Subsequently, transects were casted at a spacing of 10 m along the baseline, as shown in Fig. 2. Thereafter, the SCEs were calculated using the intersections of transects with the ToB and

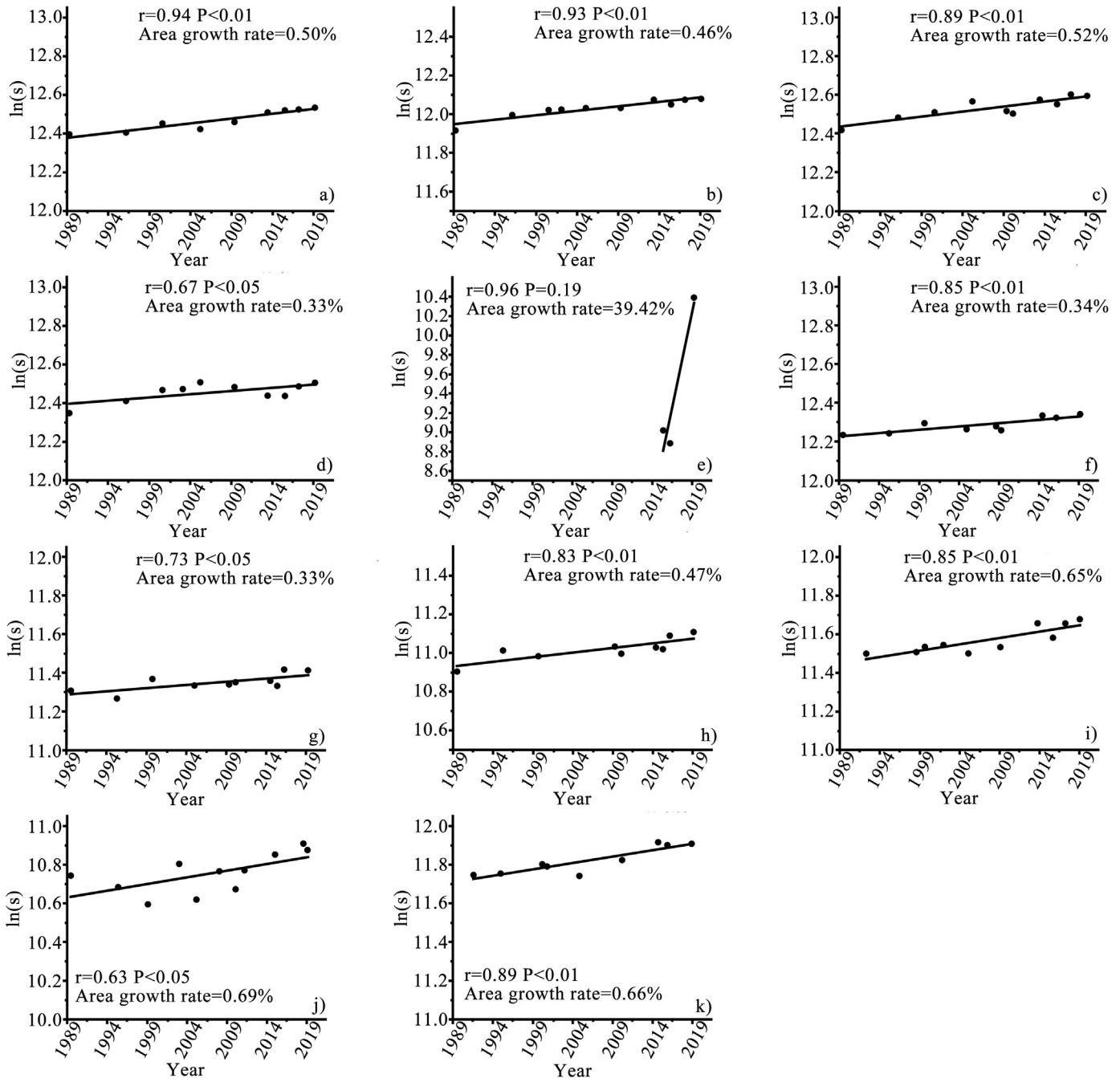


Fig. 3. Area growth rates of the vegetation on the lime-sand islands in SCS: (a) Ganquan Island; (b) Jinqing Island; (c) Jinyin Island; (d) Shanhu Island; (e) Xishazhou; (f) Bei Island; (g) Zhong Island; (h) Nan Island; (i) Beizi Island; (j) Mahuan Island; (k) Xiyue Island.

the vegetation line. Finally, the beach width was estimated using the average of the SCEs.

To calculate beach width, the baseline was created as follows: 1) A buffer was established for the vegetation line; 2) the inner boundary of the buffer was then converted to a line; 3) the line was smoothed and chosen as the baseline. Thereafter, transects were generated using the DSAS 5.0, where the transects were as perpendicular to the vegetation boundary as possible. To evaluate the influence of the baseline selection on the estimation of the beach width, two different baselines separated by 40 m were created. Results showed that the difference of the two estimated beach widths was only 0.59 m, i.e. 1.6% of the beach width or 1.5%

the distance of the two baselines. In other words, the estimation of the beach width was insensitive to the baseline selection.

### 3. Results

#### 3.1. Areal growth of vegetation on the lime-sand islands

As shown in Fig. 3, except for 39.42% per year for Xishazhou, the area growth rates of the vegetation on the lime-sand islands ranged from 0.33% to 0.69% per year during 1989 to 2019. Corresponding Pearson correlation coefficients ( $r$ ) ranged from 0.63 to 0.96. Areal expansions

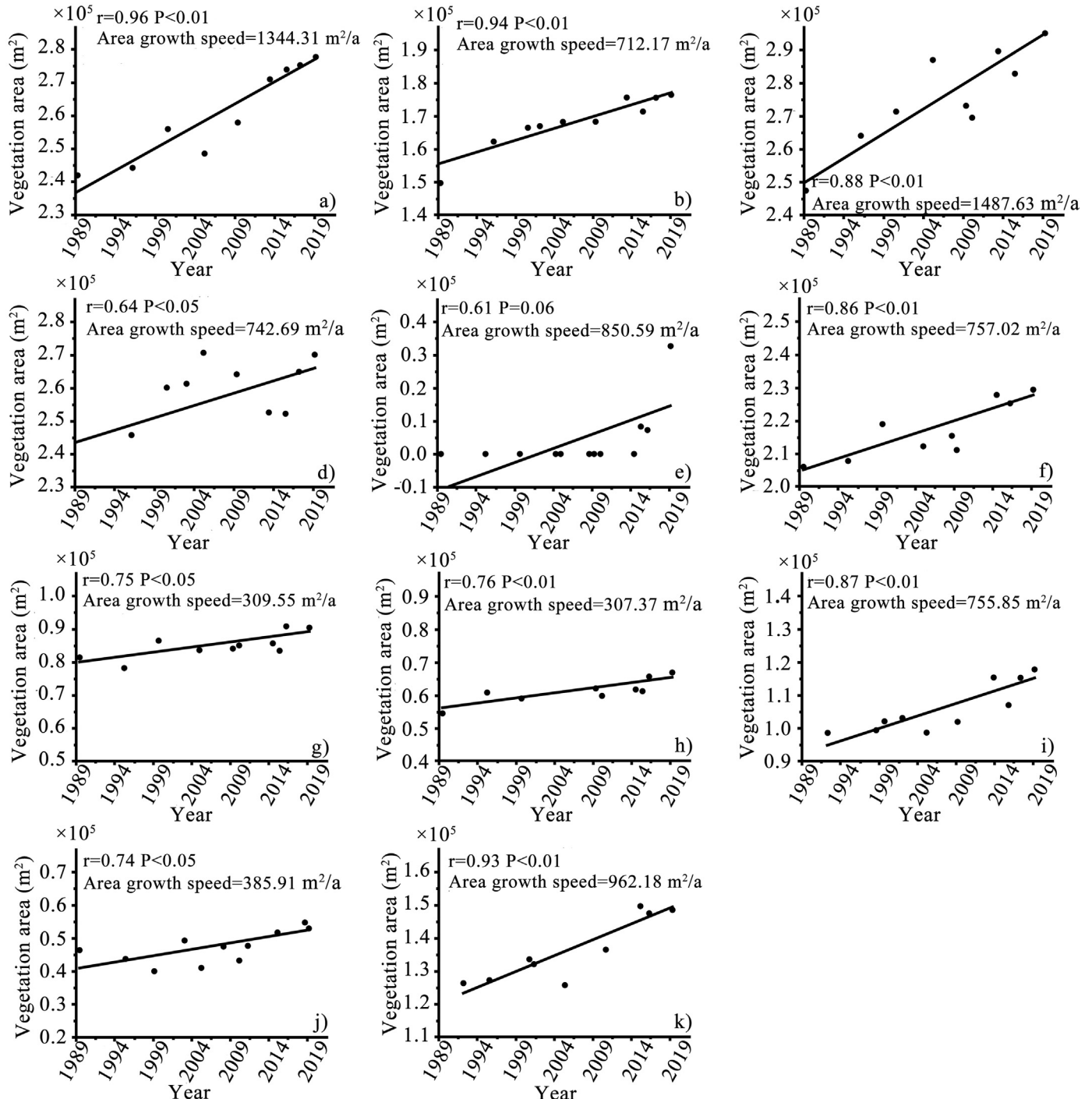


Fig. 4. As in Fig. 3, but for area growth speeds of the vegetation on the lime-sand islands in the SCS.

were also observed using vegetation area growth speeds, which were all positive (Fig. 4). The results were consistent with some previous studies such as Webb and Kench (2010), Ford (2012, 2013), Yates et al. (2013), and Ford and Kench (2014).

Note that there was no vegetation cover on Xishazhou before 2015, thus the area growth rate of its vegetation was estimated using only data from 2015 to 2019. For the same reason, it was difficult to use the area growth speed of the vegetation on Xishazhou (Fig. 4) to describe the true annual vegetation growth. Therefore, we do not discuss the area growth rate and speed of the vegetation on Xishazhou.

### 3.2. Areal decreases of the lime-sand islands

The area growth rates of the lime-sand islands are shown in Fig. 5. In contrast to the vegetation, the lime-sand island areas exhibited a

decreasing trend over the past three decades, with growth rates ranging from  $-0.60\%$  to  $-0.04\%$  per year. The results were consistent with Romine et al. (2009), Houser et al. (2014), and Thomas and Hildegard (2014). Shoreline erosions were also found from their detections of ToB/LWM and beach ridge crests.

As previously described, to study the possible influence of tidal levels on the extraction of the lime-sand island areas, we drew the extracted areas of Ganquan Island and the corresponding tidal levels on a scattergraph (Fig. 6). As shown in the figure, there was a certain correlation between the estimated areas and tidal levels; that is, if the tidal level increased by 1 m, the estimated area decreased by approximately  $5289\text{ m}^2$ . According to tidal levels calculated from the OSU Tidal Inversion Software, the tide difference of Ganquan Island was not greater than 1 m. Hence, the errors in areas estimated using the extracted ToB did not exceed  $5289\text{ m}^2$ . However, based on the area data used in

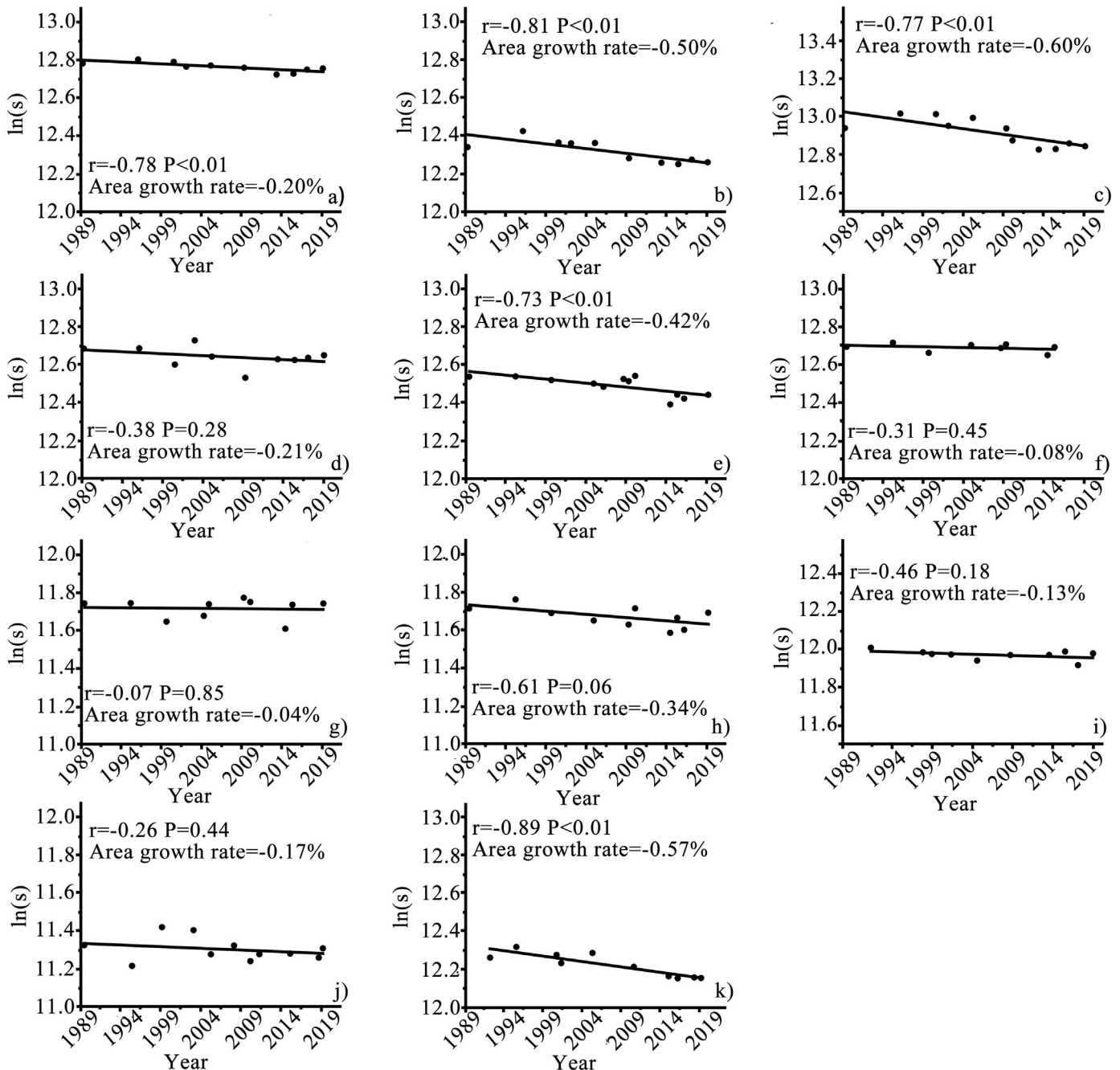


Fig. 5. As in Fig. 3, but for area growth rates of the lime-sand islands in SCS estimated using linear regression.

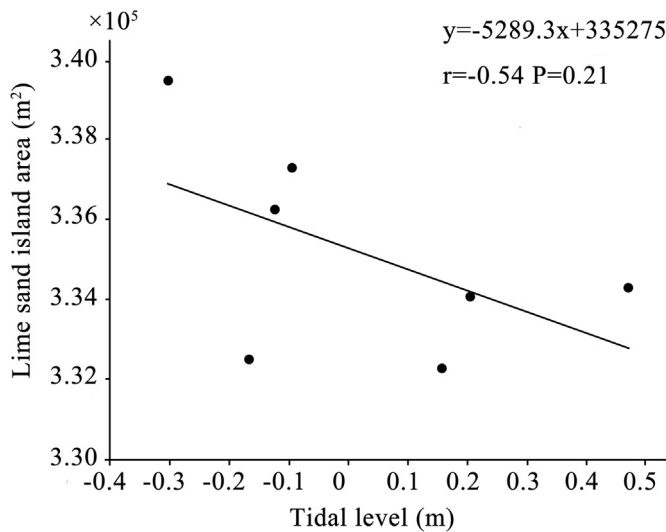


Fig. 6. Influence of the tidal level on the extracted areas of the lime-sand islands.

Fig. 5, the maximum and minimum variations in the lime-sand island areas during the study time were approximately 103,678 m<sup>2</sup> and 23,429 m<sup>2</sup>, respectively. In other words, the areal variation of a lime-sand island in the SCS was approximately 4.4 to 19.6 times greater than areal changes caused by tidal level changes. Therefore, the influences of the tide levels on the estimated lime-sand areas can be ignored.

### 3.3. Beach widths of the lime-sand islands

Beach widths were used as a bridge to combine the areas of the lime-sand islands with the vegetation for a more systematical discussion. The beach widths of the lime-sand islands in the SCS are listed in Table 2. As can be seen, the initial beach widths ranged from 31.43 to 65.66 m. Zhong Island and Jinyin Island had the narrowest and widest beaches, respectively.

## 4. Discussion

According to our results, the SCS lime-sand island areas exhibited erosion trends, whereas the vegetation tended to expand. These two key findings are not contradictory and are in fact complementary responses to climate change.

### 4.1. Response of lime-sand islands to global warming

According to the IPCC (2013), warming of the climate system is unequivocal. Sea-surface water (water depth less than 75 m) warmed by 0.11 °C per decade as a global average from 1971 to 2010. As responses to the warming, the sea-level rise has accelerated and the strongest

**Table 2**  
Beach widths of the studied lime-sand islands.

Name	Date	Width (m)
Ganquan Island	1989/04/09	57.23
Jinqing Island	1989/04/09	42.67
Jinyin Island	1989/04/09	65.66
Shanhu Island	1989/04/09	45.47
Bei Island	1989/06/20	41.77
Zhong Island	1989/06/20	31.43
Nan Island	1989/06/20	37.43
Beizi Island	1992/05/21	39.81
Mahuan Island	1989/06/15	39.48
Xiyue Island	1992/03/03	52.72

As there was no vegetation cover on Xishazhou until 2015, the beach width of Xishazhou is not listed.

tropical cyclones may be getting stronger (IPCC, 2013). Consequently, the risks of storm-surge flooding to the lime-sand islands have increased.

Since the mid-19th century, the rate of sea-level rise has been faster than the mean rate of the previous 2000 years (IPCC, 2013). According to IPCC (2013), the global sea-level rise rate during 1971 to 2010 was 2.0 mm/a. Schuerch et al. (2018) performed simulations showing that the sea level of global coastal wetland areas was projected to rise 0.29–1.10 m between 2010 and 2100 (approximately 3.2–12.2 mm/a). Here, we used a sea-level rise range of 2.0–12.2 mm/a (6.0–36.6 cm over the study period). These amounts are much lower than the tide differences in the SCS. As a result, areas of the lime-sand islands directly flooded by sea-level rise were difficult to identify from the satellite images.

However, this does not mean that the lime-sand islands have not changed due to global warming, as negative area growth rates were indeed observed (Fig. 5). Except for directly increasing the mean water depth on the reef surface, sea-level rise allowed higher wave energy to propagate to the reef surface (Sheppard et al., 2005), increasing the risk of island shoreline erosion. Furthermore, theory and modelling predicted that tropical cyclone intensity should increase with warming global mean temperatures (Emanuel, 1987; Knutson and Tuleya, 2004). Emanuel (2005) also suggested that global warming may lead to an upward trend in tropical cyclone destructive potential.

According to our grain-size analysis on two neighbouring lagoon cores from Lingyang Reef in Xisha Islands (Yue et al., 2019), the overall temporal patterns of the coarse-grained deposits (isolated coral branches and shells) from the sediment sequences were well correlated with the high sea-surface temperatures (SSTs) in the SCS. Warmer SSTs might lead to an increase in tropical cyclone intensity in the SCS. Furthermore, we downloaded typhoon data from the China Meteorological Administration (<http://tcdata.typhoon.org.cn/>), and evaluated the Strong Typhoons (STY, 41.5–50.9 m/s) and Super Typhoons (SuperTY, ≥51.0 m/s) that passed through the study area (10–20°N, 110–120°E). As shown in Fig. 7, both the annually accumulated power dissipation index (PDI) and typhoon frequency increased during 1988–2019. Furthermore, based on the Hadley Centre Sea Ice and Sea Surface Temperature data set (HadISST1) downloaded from <https://www.metoffice.gov.uk/hadobs/hadisst/data/download.html>, the SSTs around the study area have increased 0.31 °C between 1989 and 2019. As a result, we concluded that the erosion of the lime-sand islands was likely enhanced by higher wave energy and the increase in tropical cyclone intensity, both related to global warming.

On the other hand, ocean warming and acidification have caused extensive degradation of coral reefs (Hoegh-Guldberg et al., 2007; Fabricius et al., 2011). Yu (2012) indicated that the coral reefs in the SCS have been dramatically degraded with live coral cover decreasing approximately 80% from 1980 to 2008–2009. According to Qin et al. (2019), within a region of anomalously warm SSTs, the live coral cover of the Xisha Islands in the central SCS has declined from 90% during the 1980s and 1990s to 15% during the 2010s. Our previous work (Chen et al., 2019) showed that the average live coral cover in 81 study sites of the SCS fell to 16.3% in 2015. In total, the live coral cover of 46.9% of the total study sites was in the 0–20% range, whereas 21, 16.1, and 13.5% of sites had a live coral cover range of 20–30, 30–40, and 40–50%, respectively. Only 2.5% of sites had a high live coral cover of more than 50%.

It is well understood that coral reefs are crucial to maintain a stable shoreline (Yu, 2012; Ferrario et al., 2014), and as such, coral reef degradation further accelerates shoreline erosion. For example, coral communities with lower diversity and cover corresponded to more serious shoreline erosion in the Puqian Bay of Hainan Island (Zhao et al., 2019). As a result, we further considered that coral reef degradation was likely a responsible mechanism for the areal decreases of the SCS lime-sand islands.

Coral reefs can effectively dissipate incident wave energy through a combination of breaking and friction (Hearn, 1999). Meta-analyses revealed that coral reefs can provide substantial protection by reducing on average 97% of the wave energy (Ferrario et al., 2014). For this reason,

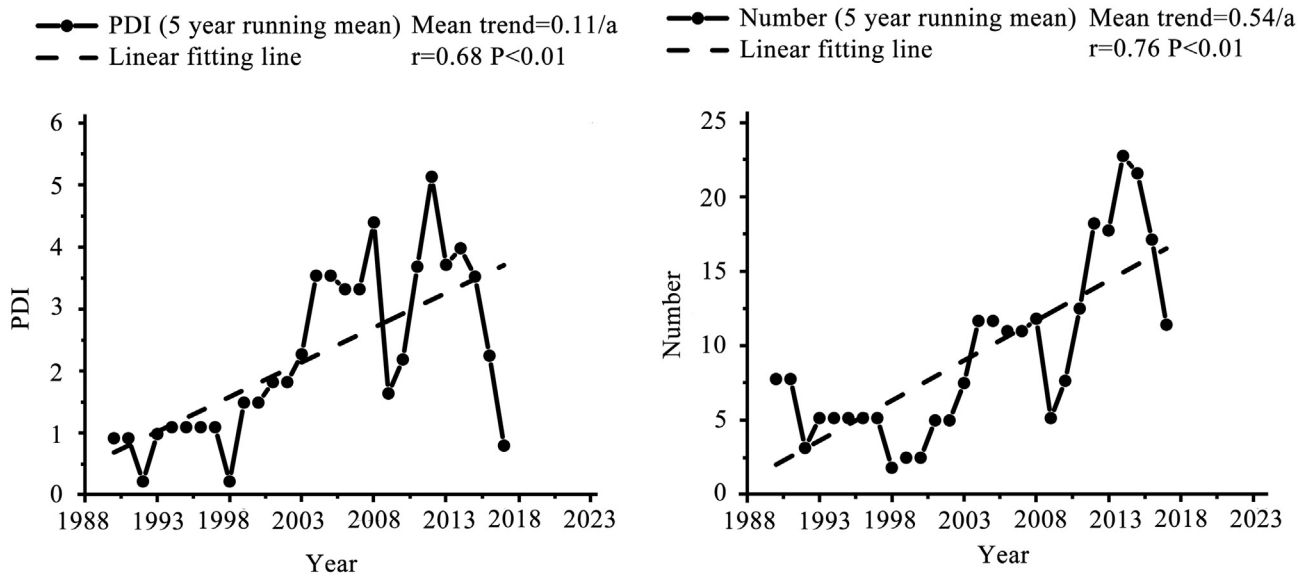


Fig. 7. Trends of annually accumulated PDI and the number of STY and SuperTY that passed through the study area.

coral reefs can fundamentally adjust the interaction between sea waves and reef-fringed shorelines (Kench and Brander, 2006a, 2006b). In other words, the degradation of coral reefs reduces bottom friction, which in turn increases wave heights, wave run-up, and wave-driven flooding (Quataert et al., 2015; Storlazzi et al., 2015). In addition, coral reef coasts are caused by one biogeomorphologic process, the result of the interactions between biological, dynamical, sedimentary, and geomorphologic processes (Naylor et al., 2002; Spencer and Viles, 2002; Zhang et al., 2006; Zhang, 2007). The material base for the biogeomorphologic process of coral reef coasts comes from the high growth rate of hermatypic coral and the high accumulation rate of the coral reefs (Naylor et al., 2002; Spencer and Viles, 2002; Zhang et al., 2006; Zhang, 2007). With the degradation of the coral reef ecosystems, the lime-sand island coasts could potentially receive less coral skeleton debris to maintain the existing area. Therefore, global-warming-caused coral reef degradation is an important factor that accelerates erosions of lime-sand islands.

In summary, direct inundation caused by sea-level rise was difficult to identify from satellite images. However, high wave energy, strong tropical cyclone intensity, and increasing tropical cyclone destructiveness caused by global warming might have greatly accelerated lime-sand island erosion. Even worse, coral reef degradation might also dramatically erode the lime-sand islands. Synthetic effects of these factors were enough to make the area changes of the lime-sand islands become significant in the experimental satellite images. Area decreases of the lime-sand islands extracted from the satellite images corresponded to these conclusions.

4.2. Response of lime-sand island vegetation to global warming

In contrast to the island areal trends, vegetation on the SCS lime-sand islands expanded over time (Figs. 3 and 4). This is in accordance with other vegetation area studies. Webb and Kench (2010) found that 86% of the vegetation on 27 lime-sand islands in the central Pacific Ocean remained stable or increased; Ford (2013) observed that the vegetation of 32 of 49 lime-sand islands in the Wotje Atoll of the Marshall Islands increased in area from 1945 to 2010; and Ford and Kench (2015) showed that the vegetation on six atolls and two lime-sand islands in the Marshall Islands expanded between 1943 and 2010. These results do not contradict with the erosion of the SCS lime-sand islands; in fact, they are further evidence of climate change impacts.

According to Li et al. (2018), the temperature around the Xisha Islands increased approximately 0.019 °C/a. As the SST continued to rise, evaporation increased, resulting in an increase in atmospheric humidity. In turn, higher humidity can promote increased precipitation (Bretherton et al., 2004; Rushley et al., 2018). Smith et al. (2006)

showed concomitant precipitation and SST increases in the western tropical Pacific. In addition, Xisha Islands precipitation exhibited an upward trend of approximately 3.18 mm/a from 1959 to 2014 (Li et al., 2018). As precipitation increases are generally conducive to vegetation growth, the observed vegetation expansion on the lime-sand islands in the SCS may be the result.

To examine changes in vegetation and how they relate to precipitation trends, we investigated the differences between the vegetation growth rates of islands in the central and southern SCS. According to Chen et al. (2018), both the central and southern SCS exhibit a positive SST-precipitation correlation, but the SST-precipitation correlation over the central SCS is weaker. Therefore, climate change related increases in southern SCS precipitation are likely greater than those in the central SCS. As a result, vegetation growth rates in the southern SCS should be greater than in the central SCS. This was demonstrated by our satellite images, as the vegetation growth rates on Mahuan Island, Xiyue Island, and Beizi Island were greater than those on Ganquan Island, Jinyin Island, Shanhu Island, Jinqing Island, Bei Island, Zhong Island, and Nan Island.

4.3. How vegetation and beaches have affected the lime-sand islands under global warming

The erosion of the lime-sand islands and the vegetation expansion were associated with site-specific conditions, such as initial vegetation and beach widths. For example, the area growth speed of the vegetation was positively correlated with the initial vegetation areas and beach width, whereas the area growth rate of the lime-sand islands was negatively correlated with initial beach width (Fig. 8). Here, the initial vegetation area represented the vegetation area on a lime-sand island at the beginning of the study period.

The slope shown in Fig. 8a is the average area growth rate of the vegetation on the lime-sand islands in the SCS. Specifically, 1 m<sup>2</sup> of initial vegetation can produce roughly 0.0042 m<sup>2</sup> of new vegetation per year. In other words, the larger the initial vegetation area, the larger the vegetation area growth speed will be. In general, the vegetation perimeter is larger on a lime-sand island with a large vegetation area. As a result, the opportunity for the vegetation to expand outward is greater.

Note that the spaces for the vegetation to expand are mainly on the beaches. Therefore, the vegetation area growth speed should also be related to beach width. This was verified by performing a linear regression of the vegetation area growth speeds on the initial beach widths (Fig. 8b). The slope indicates that if the initial beach width of a lime-sand island increases by 1 m, the vegetation area growth speed will

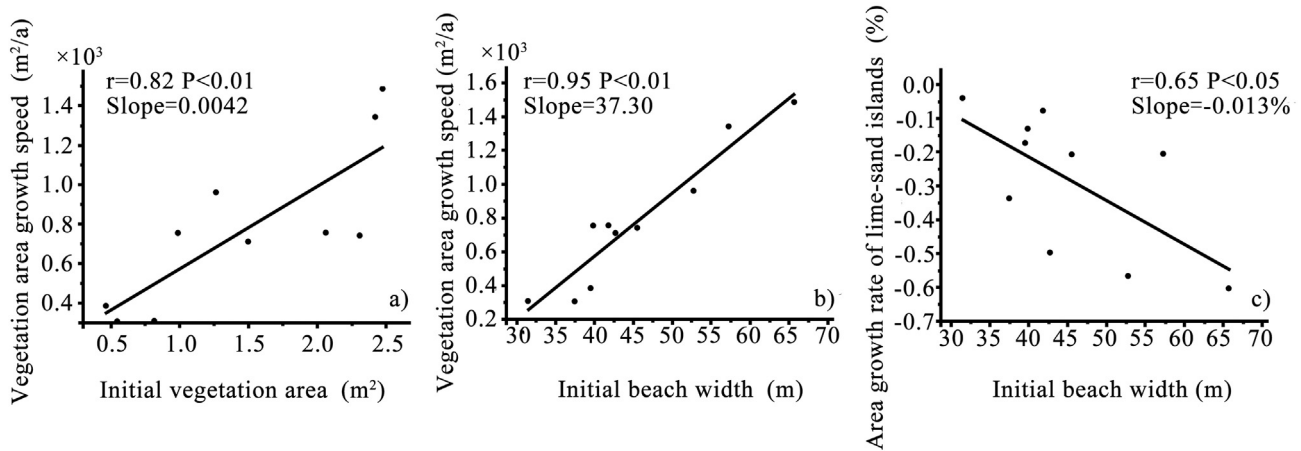


Fig. 8. Schematic diagram of linear regressions. (a) Linear regression of the vegetation area growth speed on the initial vegetation areas. (b) Linear regression of the vegetation area growth speeds on the initial beach widths. (c) Linear regression of the lime-sand island area growth rates on the initial beach widths.

increase by 37.3 m<sup>2</sup>/a. In fact, the wider the beach width, the farther the vegetation is from the edge of the lime-sand island, and the less affected the vegetation will be by the seawater, ensuring that it will grow more. As an extreme case example, Xishazhou had no vegetation cover until 2015. However, once the vegetation formed, vegetation growth was fast, as shown in Figs. 3 and 4.

Growth rates of the lime-sand islands in the SCS were negatively correlated with initial beach widths (Fig. 8c). The slope shows that if the initial beach width increased by 1 m, the area growth rate decreased by 0.013%. In other words, the lime-sand islands with narrow beaches exhibited stronger stability than those with broad beaches.

As a lime-sand island in SCS can be generally divided into the vegetation and the beach, we can infer from Fig. 8c that the erosion rates of the lime-sand islands declined with vegetation expansion. In other words, the vegetation played an important role in preventing sand/sediment erosion caused by tropical cyclone flooding or high wave energy. This was also why areal decrease rates fell as beach widths became narrow.

4.4. How the lime-sand islands will change under global warming

In summary, inundation directly caused by sea-level rise could not be directly observed from satellite images over the past 30 years, but island

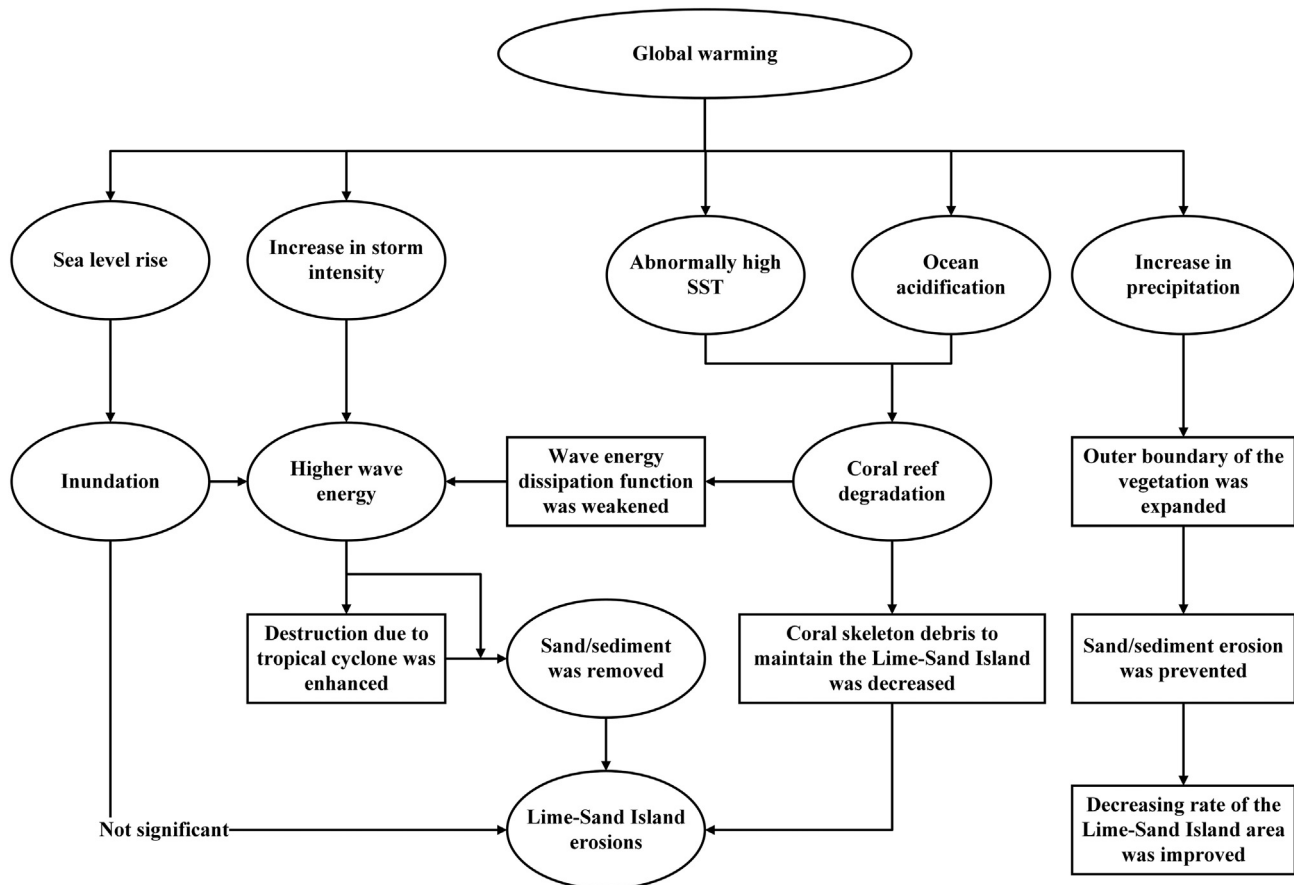


Fig. 9. Summary of the responses of the lime-sand islands in the SCS to global warming.

erosions were well-detected. Based on previous analysis, these erosions were caused by higher wave energy, stronger typhoon intensity, and more serious tropical cyclone destructiveness. Erosion increased due to the degradation of coral reefs resulting from global warming. In contrast, vegetation expanded, likely due to regional precipitation increases associated with climate change. According to previous discussions, the expansions were due to increase of precipitation caused by global warming in central and southern SCS. In addition, site-specific conditions of the lime-sand islands, such as initial vegetation and beach widths, impacted erosion and vegetation expansion rates. The potential impacts of global warming on these islands are summarised in Fig. 9.

Overall, the lime-sand island vegetation area in the SCS should continue to increase due to increasing precipitation. Meanwhile, the lime-sand islands may continue to erode under climate change. Therefore, the beach width of a lime-sand island in the SCS will narrow until the edge of the vegetation is close enough to the seawater. During the approach, both the growth rates of the vegetation and the decrease rates of the lime-sand islands may become smaller and smaller over time (Fig. 8b and c).

However, if the vegetation is adjacent to the seawater, vegetation growth will be significantly inhibited (Rozema and Diggelen, 1991). As a result, the vegetation may decrease once it expands to the seawater. In that case, the lime-sand islands may further erode. In sum, both the lime-sand islands and their respective vegetation areas should continually decline under further global warming.

## 5. Conclusions

To help understand how lime-sand islands are changing due to global warming, changes in island and vegetation areas in the SCS were detected using a series of Landsat MSS, TM, ETM+, OLI, and Sentinel-2 MSI images (1989–2019). Area growth rates and speeds were used to quantitatively analyse the changes in the lime-sand islands and their vegetation. Results showed that lime-sand islands in the SCS have eroded, whereas their vegetation has expanded.

Our analysis showed that direct inundation caused by sea-level rise in the SCS could not be significantly identified from satellite images. However, other global-warming-related factors such as higher wave energy, stronger typhoon intensity, and severe tropical cyclone destructiveness could potentially exacerbate shoreline erosions. Furthermore, global warming has accelerated the degradation of the coral reefs around the lime-sand islands, which may have exacerbated shoreline erosions. Synthetic effects of these factors made the decline in island area to appear quite significant in the satellite images. In contrast, vegetation expansion on the lime-sand islands was caused by the increase in regional precipitation related to warmer SSTs and increased evaporation. Based on our results, we concluded how lime-sand islands may evolve with global warming: 1) the islands will continue to erode and the vegetation will continue to expand; 2) vegetation growth will be significantly inhibited by saline water and vegetation area will start to decrease if the vegetation becomes adjacent to the seawater.

As the changes in area of the lime-sand islands and their vegetation were observed to agree with the analytical results, this study showed that satellite remote sensing can be regarded as an evidence on how the lime-sand islands have responded to global warming over the past several decades. This study was the first to quantitatively assess the changes to the lime-sand islands in the SCS. Our results can further help understand how lime-sand islands will respond to future global warming across the world.

## Declaration of competing interest

The authors declare that they have no known competing financial interests or personal relationships that could have appeared to influence the work reported in this paper.

## Acknowledgments

This work was financially supported by the Natural Science Foundation of China (Nos. 91428203 and 41766007), Guangxi scientific projects (Nos. AD17129063 and AA17204074), Guangxi Innovative Development Grand Grant (No. AA18118038), and Key Special Project for Introduced Talents Team of Southern Marine Science and Engineering Guangdong Laboratory (Guangzhou) (No. GML2019ZD0302).

## Data availability

Experimental Landsat MSS, TM, ETM+, OLI, and Sentinel-2 MSI imagery can be downloaded from the United States Geological Survey (USGS) website (<https://earthexplorer.usgs.gov/>), and the tidal levels can be calculated by using the Oregon State University (OSU) Tidal Inversion Software (<http://volkov.oce.orst.edu/tides/>).

## References

- Barnett, J., 2005. Titanic states? Impacts and responses to climate change in the Pacific islands. *J. Int. Aff.* 59, 203–219. <https://doi.org/10.1002/0470024747.ch10>.
- Behling, R., Milewski, R., Chabrilat, S., 2018. Spatiotemporal shoreline dynamics of Namibian coastal lagoons derived by a dense remote sensing time series approach. *Int. J. Appl. Earth Obs.* 68, 262–271. <https://doi.org/10.1016/j.jag.2018.01.009>.
- Bretherton, C.S., Peters, M.E., Back, L.E., 2004. Relationships between water vapor path and precipitation over the tropical oceans. *J. Clim.* 17, 1517–1528. [https://doi.org/10.1175/1520-0442\(2004\)017<1517:RBVWPA>2.0.CO;2](https://doi.org/10.1175/1520-0442(2004)017<1517:RBVWPA>2.0.CO;2).
- Burke, L., Selig, E., Spalding, M., 2002. *Reefs at Risk in Southeast Asia*. World Resources Inst., Washington D.C.
- Chen, X., Vierling, L., Deering, D., 2005. A simple and effective radiometric correction method to improve landscape change detection across sensors and across time. *Remote Sens. Environ.* 98, 63–79. <https://doi.org/10.1016/j.rse.2005.05.021>.
- Chen, J., Wang, X., Zhou, W., Wen, Z., 2018. Interdecadal change in the summer SST-precipitation relationship around the late 1990s over the South China Sea. *Clim. Dyn.* 51, 2229–2246. <https://doi.org/10.1007/s00382-017-4009-y>.
- Chen, X., Yu, K., Huang, X., Wang, Y., Liao, Z., Zhang, R., Yao, Q., Wang, J., Wang, W., Tao, S., Zhang, H., 2019. Atmospheric nitrogen deposition increases the possibility of macroalgal dominance on remote coral reefs. *J. Geophys. Res.: Biogeosciences* 124, 1355–1369. <https://doi.org/10.1029/2019JG005074>.
- Cheng, J., Foo, S.W., 2007. Distraction in GVF-based segmentation. 6th International Conference on Information, Communications & Signal Processing, pp. 1–4. <https://doi.org/10.1109/ICIS.2007.4449682>.
- Clayton, D.G., 1971. Algorithm AS 46: Gram-schmidt orthogonalization. *J. R. Stat. Soc. Ser. C Appl. Stat.* 20, 335–338.
- Connell, J., 2003. Losing ground? Tuvalu, the greenhouse effect and the garbage can. *Asia Pac. Viewp.* 44, 89–107. <https://doi.org/10.1111/1467-8373.00187>.
- Cooley, T., Anderson, G.P., Felde, G.W., Hoke, M.L., Ratkowski, A.J., Chetwynd, J.H., Gardner, J.A., Adler-Golden, S.M., Matthew, M.W., Berk, A., Bernstein, L.S., Acherya, P.K., Miller, D., Lewis, P., 2002. FLAASH, a MODTRAN4-based atmospheric correction algorithm, its application and validation. IEEE International Geoscience and Remote Sensing Symposium. <https://doi.org/10.1109/igars.2002.1026134>.
- Deng, W., Wei, G., Xie, L., Ke, T., Wang, Z., Zeng, T., Liu, Y., 2013. Variations in the Pacific Decadal Oscillation since 1853 in a coral record from the northern South China Sea. *J. Geophys. Res.: Oceans* 118, 2358–2366. <https://doi.org/10.1002/jgrc.20180>.
- Dickinson, W.R., 2009. Pacific atoll living: how long already and until when. *Geol. Soc.* 19, 4–10. <https://doi.org/10.1130/GSATG35A.1>.
- Emanuel, K.A., 1987. The dependence of hurricane intensity on climate. *Nature* 326, 483–485. <https://doi.org/10.1038/326483a0>.
- Emanuel, K.A., 2005. Increasing destructiveness of tropical cyclones over the past 30 years. *Nature* 436, 686–688. <https://doi.org/10.1038/nature03906>.
- Erkol, B., Moss, R.H., Stanley, R.J., Stoecker, W.V., Hvatum, E., 2010. Automatic lesion boundary detection in dermoscopy images using gradient vector flow snakes. *Skin Res. Technol.* 11, 17–26. <https://doi.org/10.1111/j.1600-0846.2005.00092.x>.
- Fabrizius, K.E., Langdon, C., Uthicke, S., Humphrey, C., Noonan, S., De'ath, G., Okazaki, R., Muehllehner, N., Glas, M.S., Lough, J.M., 2011. Losers and winners in coral reefs acclimatized to elevated carbon dioxide concentrations. *Nat. Clim. Chang.* 1, 165–169. <https://doi.org/10.1038/nclimate1122>.
- Ferrario, F., Beck, M.W., Storlazzi, C.D., Micheli, F., Shepard, C.C., Airoidi, L., 2014. The effectiveness of coral reefs for coastal hazard risk reduction and adaptation. *Nat. Commun.* 5, 3794. <https://doi.org/10.1038/ncomms4794>.
- Fletcher, C., Rooney, J., Barbee, M., Lim, S., Richmond, B., 2003. Mapping shoreline change using digital orthophotogrammetry on Maui, Hawaii. *J. Coast. Res.* 19, 106–124.
- Ford, M.R., 2012. Shoreline changes on an urban atoll in the central Pacific Ocean: Majuro Atoll, Marshall Islands. *J. Coast. Res.* 28, 11–22. <https://doi.org/10.2112/JCOASTRES-D-11-00008.1>.
- Ford, M.R., 2013. Shoreline changes interpreted from multi-temporal aerial photographs and high resolution satellite images: Wotje Atoll, Marshall Islands. *Remote Sens. Environ.* 135, 130–140. <https://doi.org/10.1016/j.rse.2013.03.027>.
- Ford, M.R., Kench, P.S., 2014. Formation and adjustment of typhoon-impacted reef islands interpreted from remote imagery: Nadikdik Atoll, Marshall Islands. *Geomorphology* 214, 216–222. <https://doi.org/10.1016/j.geomorph.2014.02.006>.

- Ford, M.R., Kench, P.S., 2015. Multi-decadal shoreline changes in response to sea level rise in the Marshall Islands. *Anthropocene* 11, 14–24. <https://doi.org/10.1016/j.ancene.2015.11.002>.
- Haque, M.M., Ahmed, F., Anam, S., Kabir, M.R., 2012. Future population projection of Bangladesh by growth rate modeling using logistic population model. *Ann. Pure Appl. Logic* 1, 192–202.
- Hearn, C.J., 1999. Wave-breaking hydrodynamics within coral reef systems and the effect of changing relative sea level. *J. Geophys. Res.* 104, 30007–30019. <https://doi.org/10.1029/1999jc000262>.
- Himmelstoss, E.A., Henderson, R.E., Kratzmann, M.G., Farris, A.S., 2018. *Digital Shoreline Analysis System (DSAS) version 5.0 user guide*. U.S. Geological Survey Open-File Report 2018-1179 (110 pp).
- Hoegh-Guldberg, O., Mumby, P.J., Hooten, A.J., Steneck, R.S., Greenfield, P., Gomez, E., Harvell, C.D., Sale, P.F., Edwards, A.J., Caldeira, K., Knowlton, N., Eakin, C.M., Iglesias-Prieto, R., Muthiga, N., Bradbury, R.H., Dubi, A., Hatzioiols, M.E., 2007. Coral reefs under rapid climate change and ocean acidification. *Science* 318, 1737–1742. <https://doi.org/10.1126/science.1152509>.
- Houser, C., D'Ambrosio, T., Bouchard, C., Heyman, W., Darbonne, K., Kuykendall, S., 2014. Erosion and reorientation of the Sapodilla Cays, Mesoamerican Reef Belize from 1960 to 2012. *Phys. Geogr.* 35, 335–354. <https://doi.org/10.1080/02723646.2014.913932>.
- Huang, R., Yu, K., Wang, Y., Wang, J., Mu, L., Wang, W., 2017. Bathymetry of the coral reefs of Weizhou Island based on multispectral satellite images. *Remote Sens.* 9, 750. <https://doi.org/10.3390/rs9070750>.
- Huang, R., Yu, K., Wang, Y., Wang, W., Mu, L., Wang, J., 2018. Method to design a live coral cover sensitive index for multispectral satellite images. *Opt. Express* 26, A374–A397. <https://doi.org/10.1364/OE.26.00A374>.
- IPCC, 2013. Summary for policymakers. In: Stocker, T.F., Qin, D., Plattner, G.-K., et al. (Eds.), *Climate Change 2013: The Physical Science Basis. Contribution of Working Group I to the Fifth Assessment Report of the Intergovernmental Panel on Climate Change*, pp. 1–29.
- IPCC, 2018. Summary for policymakers. In: Masson-Delmotte, V., Zhai, P., Pörtner, H.-O., Roberts, D., Skea, J., Shukla, P.R., Pirani, A., Moufouma-Okia, W., Péan, C., Pidcock, R., Connors, S., Matthews, J.B.R., Chen, Y., Zhou, X., Gomis, M.I., Lonnoy, E., Maycock, T., Tignor, M., Waterfield, T. (Eds.), *Global Warming of 1.5 °C. An IPCC Special Report on the Impacts of Global Warming of 1.5°C Above Pre-industrial Levels and Related Global Greenhouse Gas Emission Pathways, in the Context of Strengthening the Global Response to the Threat of Climate Change, Sustainable Development, and Efforts to Eradicate Poverty*, pp. 1–24.
- Kass, M., Witkin, A., Terzopoulos, D., 1988. Snakes: active contour models. *Int. J. Comput. Vis.* 1, 321–331. <https://doi.org/10.1007/BF00133570>.
- Kench, P.S., Brander, R.W., 2006a. Response of reef island shorelines to seasonal climate oscillations: South Maalhosmadulu Atoll, Maldives. *J. Geophys. Res. Earth Surf.* 111 (F01001). <https://doi.org/10.1029/2005JF000323>.
- Kench, P.S., Brander, R.W., 2006b. Wave processes on coral reef flats: implications for reef geomorphology using Australian case studies. *J. Coast. Res.* 221, 209–223. <https://doi.org/10.2112/05A-0016.1>.
- Knutson, T.R., Tuleya, R.E., 2004. Impact of CO<sub>2</sub>-induced warming on simulated hurricane intensity and precipitation: sensitivity to the choice of climate model and convective parameterization. *J. Climate* 17, 3477–3495. [https://doi.org/10.1175/1520-0442\(2004\)017<3477:IOCWOS>2.0.CO;2](https://doi.org/10.1175/1520-0442(2004)017<3477:IOCWOS>2.0.CO;2).
- Kossin, J.P., Olander, T.L., Knapp, K.R., 2013. Trend analysis with a new global record of tropical cyclone intensity. *J. Clim.* 26, 9960–9976. <https://doi.org/10.1175/JCLI-D-13-00262.1>.
- Kossin, J.P., Knapp, K.R., Olander, T.L., Velden, C.S., 2020. Global increase in major tropical cyclone exceedance probability over the past four decades. *Proc. Natl. Acad. Sci.* 117, 11975–11980. <https://doi.org/10.1073/pnas.1920849117>.
- Li, J., Bai, A., Cai, Q., 2018. Climate change characteristics of the Xisha Islands and Weizhou Island in China and the comparison with the coastal land. *J. Trop. Geogr.* 38, 72–81. <https://doi.org/10.13284/j.cnki.rddl.003003>.
- Liu, J., Chen, Z., Chen, M., Yan, W., Xiang, R., Tang, X., 2010. Magnetic susceptibility variations and provenance of surface sediments in the South China Sea. *Sediment. Geol.* 230, 77–85. <https://doi.org/10.1016/j.sedgeo.2010.07.001>.
- Liu, J., Huang, R., Yu, K., 2020. Analysis on the geomorphic changes of Huangyan Island based on satellite images over the past 40 years. *J. Quat. Sci.* 40, 775–790. <https://doi.org/10.11928/j.issn.1001-7410.2020.03.15>.
- McAdam, J., 2010. 'Disappearing states', statelessness and the boundaries of international law. UNSW Law Research Paper 2, 1–23.
- McLean, R., Kench, P., 2015. Destruction or persistence of coral atoll islands in the face of 20th and 21st century sea-level rise? *Wiley Interdiscip. Rev. Clim. Chang.* 6, 445–463. <https://doi.org/10.1002/wcc.350>.
- Mimura, N., 1999. Vulnerability of island countries in the south Pacific to sea level rise and climate change. *Clim. Res.* 12, 137–143. <https://doi.org/10.3354/cr012137>.
- Morton, B., Blackmore, G., 2001. South China Sea. *Mar. Pollut. Bull.* 42, 1236–1263. [https://doi.org/10.1016/S0025-326X\(01\)00240-5](https://doi.org/10.1016/S0025-326X(01)00240-5).
- National Marine Information Center, 2017. Marine bulletin. <http://www.nmdis.org.cn/gongbao/>. (Accessed 10 December 2019).
- Naylor, L.A., Viles, H.A., Carter, N.E.A., 2002. Biogeomorphology revisited: looking towards the future. *Geomorphology* 47, 3–14. [https://doi.org/10.1016/S0169-555X\(02\)00137-X](https://doi.org/10.1016/S0169-555X(02)00137-X).
- Qin, Z., Yu, K., Wang, Y., Xu, L., Huang, X., Chen, B., et al., 2019. Spatial and intergeneric variation in physiological indicators of corals in the South China Sea: insights into their current state and their adaptability to environmental stress. *J. Geophys. Res.: Oceans* 124, 3317–3332. <https://doi.org/10.1029/2018JC014648>.
- Quataert, E., Storlazzi, C., Rooijen, A.V., Cheriton, O., Dongeren, A.V., 2015. The influence of coral reefs and climate change on wave-driven flooding of tropical coastlines. *Geophys. Res. Lett.* 42, 6407–6415. <https://doi.org/10.1002/2015GL064861>.
- Romine, B.M., Fletcher, C.H., 2013. A summary of historical shoreline changes on beaches of Kauai, Oahu, and Maui. *Hawaii. J. Coast. Res.* 29, 605–614. <https://doi.org/10.2112/JCOASTRES-D-11-00202.1>.
- Romine, B.M., Fletcher, C.H., Frazer, L.N., Genz, A.S., Barbee, M.M., Lim, S., 2009. Historical shoreline change, Southeast Oahu, Hawaii: applying polynomial models to calculate shoreline change rates. *J. Coast. Res.* 25, 1236–1253. <https://doi.org/10.2112/08-1070.1>.
- Rozeema, J., Diggelen, J.V., 1991. A comparative study of growth and photosynthesis of four halophytes in response to salinity. *Acta Oecol.* 12, 673–681.
- Rushley, S.S., Kim, D., Bretherton, C.S., Ahn, M.-S., 2018. Reexamining the nonlinear moisture-precipitation relationship over the tropical oceans. *Geophys. Res. Lett.* 45, 1133–1140. <https://doi.org/10.1002/2017gl076296>.
- Schuerch, M., Spencer, T., Temmerman, S., Kirwan, M.L., Wolff, C., Lincke, D., McOwen, C.J., Pickering, M.D., Reef, R., Vafeidis, A.T., Hinkel, J., Nicholls, R.J., Brown, S., 2018. Future response of global coastal wetlands to sea-level rise. *Nature* 561, 231–234. <https://doi.org/10.1038/s41586-018-0476-5>.
- Sheppard, C., Dixon, D.J., Gourlay, M., Sheppard, C., Payet, R., 2005. Coral mortality increases wave energy reaching shores protected by reef flats: examples from the Seychelles. *Estuar. Coast. Shelf Sci.* 64, 223–234. <https://doi.org/10.1016/j.ecss.2005.02.016>.
- Smith, T.M., Yin, X., Gruber, A., 2006. Variations in annual global precipitation (1979–2004), based on the global precipitation climatology project 2.5° analysis. *Geophys. Res. Lett.* 33, L06705. <https://doi.org/10.1029/2005GL025393>.
- Song, X., Tang, G., Li, F., Jiang, L., Zhou, Y., Qian, K., 2013. Extraction of loess shoulder-line based on the parallel GVF snake model in the loess hilly area of China. *Comput. Geosci.* 52, 11–20. <https://doi.org/10.1016/j.cageo.2012.08.014>.
- Spencer, T., Viles, H., 2002. Bioconstruction, bioerosion and disturbance on tropical coasts: coral reefs and rocky limestone shores. *Geomorphology* 48, 23–50. [https://doi.org/10.1016/S0169-555X\(02\)00174-5](https://doi.org/10.1016/S0169-555X(02)00174-5).
- Stoddart, D.R., Steers, J.A., 1977. The nature and origin of coral reef islands. In: Jones, O.A., Endean, R. (Eds.), *Biology and Geology of Coral Reefs*. vol. 4. Academic Press, New York, pp. 59–105. <https://doi.org/10.1016/B978-0-12-395528-9.50011-7>.
- Storlazzi, C.D., Elias, E.P.L., Berkowitz, P., 2015. Many atolls may be uninhabitable within decades due to climate change. *Sci. Rep.* 5, 14546. <https://doi.org/10.1038/srep14546>.
- Talau-McManus, L., 2000. *Transboundary diagnostic analysis for the South China Sea*. EAS/RCU Technical Report Series Number 14. UNEP, Bangkok, Thailand.
- Terry, J.P., Chui, T.F.M., 2012. Evaluating the fate of freshwater lenses on atoll islands after eustatic sea-level rise and cyclone-driven inundation: a modelling approach. *Glob. Planet. Chang.* 88–89, 76–84. <https://doi.org/10.1016/j.gloplacha.2012.03.008>.
- Thomas, M., Hildegard, W., 2014. Assessing long-term changes in the beach width of reef islands based on temporally fragmented remote sensing data. *Remote Sens.* 6, 6961–6987. <https://doi.org/10.3390/rs6086961>.
- Webb, A.P., Kench, P.S., 2010. The dynamic response of reef islands to sea-level rise: evidence from multi-decadal analysis of island change in the central pacific. *Glob. Planet. Chang.* 72, 234–246. <https://doi.org/10.1016/j.gloplacha.2010.05.003>.
- Woodroffe, C.D., 2008. Reef-island topography and the vulnerability of atolls to sea-level rise. *Glob. Planet. Chang.* 62, 77–96. <https://doi.org/10.1016/j.gloplacha.2007.11.001>.
- Xu, C., Prince, J.L., 1997. Gradient vector flow: a new external forces for snakes. *Proceedings of IEEE international conference on CVPR*. <https://doi.org/10.1109/CVPR.1997.609299>.
- Xu, L., Jackowski, M., Goshdasby, A., Roseman, D., Bines, S., Yu, C., Dhawan, A., Huntley, A., 1999. Segmentation of skin cancer images. *Image Vis. Comput.* 17, 65–74. [https://doi.org/10.1016/S0262-8856\(98\)00091-2](https://doi.org/10.1016/S0262-8856(98)00091-2).
- Yates, M.L., Cozannet, G.L., Garcin, M., Salaï, E., Walker, P., 2013. Multidecadal atoll shoreline change on Manihi and Manuae, French Polynesia. *J. Coast. Res.* 29, 870–882. <https://doi.org/10.2307/23486557>.
- Yu, K., 2012. Coral reefs in the South China Sea: their response to and records on past environmental changes. *Sci China Earth Sci.* 55, 1217–1229. <https://doi.org/10.1007/s11430-012-4449-5>.
- Yue, Y., Yu, K., Tao, S., Zhang, H., Liu, G., Wang, N., Jiang, W., Fan, T., Lin, W., Wang, Y., 2019. 3500-year western Pacific storm record warns of additional storm activity in a warming warm pool. *Palaeogeogr. Palaeoclimatol. Palaeoecol.* 521, 57–71. <https://doi.org/10.1016/j.palaeo.2019.02.009>.
- Zamani, F., Safabakhsh, R., 2007. An unsupervised GVF snake approach for white blood cell segmentation based on nucleus. *International Conference on Signal Processing*. <https://doi.org/10.1109/ICOSP.2006.345648>.
- Zhang, Q., 2007. Responses of tropical biological coasts to global change. *Quat. Sci.* 27, 834–844.
- Zhang, Q., Shi, Q., Yu, K., Zhao, M., 2006. Biogeomorphologic process of tropical biological coasts of south China. *Quat. Sci.* 26, 451–455.
- Zhang, X., Dong, G., Xiong, B., Kuang, G., 2017. Refined segmentation of ship target in SAR images based on GVF snake with elliptical constraint. *Remote Sens. Lett.* 8, 791–800. <https://doi.org/10.1080/2150704X.2017.1327124>.
- Zhao, M., Zhang, H., Zhong, Y., Jiang, D., Liu, G., Yan, H., Zhang, H., Guo, P., Li, C., Yang, H., Chen, T., Wang, R., 2019. The status of coral reefs and its importance for coastal protection: a case study of northeastern Hainan Island, South China Sea. *Sustainability* 11 (16), 4354. <https://doi.org/10.3390/su11164354>.